# Mixed-Phase $W_xMo_yC_zS_2$ Nanotubes

W. K. Hsu,[†] Y. Q. Zhu,[†] C. B. Boothroyd,[‡] I. Kinloch,[‡] S. Trasobares,[§] H. Terrones,[∥] N. Grobert,[†] M. Terrones,[⊥] R. Escudero,[#] G. Z. Chen,[‡] C. Colliex,[§] A. H. Windle,[‡] D. J. Fray,[‡] H. W. Kroto,[†] and D. R. M. Walton*[,†]

*School of Chemistry, Physics and Environmental Science, University of Sussex, Brighton BN1 9QJ, United Kingdom, Department of Materials Science and Metallurgy, University of Cambridge, Pembroke Street, Cambridge CB2 3QZ, United Kingdom, Laboratoire de Physique des Solides, Université Paris-Sud, Bâtiment 510, 91405 Orsay, France, Instituto de Física, UNAM, AP 1-1010, 76000, Querétaro, México, Max Planck Institut für Metallforschung, Seestr., 92, D-70174 Stuttgart, Germany, and Instituto de Investigaciones en Materiales, UNAM, AP 70-360, D.F. 01000, México*

*Received July 4, 2000*
*Revised Manuscript Received August 28, 2000*

Owing to their unique properties, structurally robust carbon nanotubes constitute a new class of electronic and mechanical materials.[1,2] The introduction of topological variations (e.g., heptagon−pentagon pairs)[3,4] or elements other than carbon[5] to form discrete heterostructural domains within the nanotubes has now become a key issue. Recently, well-separated BN−C-layered tubules[6,7] and multielement, for example, SiC−$SiO_2$−BN−C nanostructures,[8] have been produced by arc discharge and laser ablation techniques. Assigning their distinctive lattice constants and devising processes for generating heterostructures, however, may have limitations. Nevertheless, Hu et al. have demonstrated a rectifying effect by connecting a carbon nanotube to a silicon nanowire via chemical vapor deposition (CVD).[9] This technique provides an innovative method for generating a nanojunction diode, thus paving the way to fabricating photolithographs which form a basis for current technology in the semiconductor industry. Other layered nanomaterials with fullerene-like structures, for example, $WS_2$ or $MoS_2$, have also been produced[10,11] and their electronic properties evaluated.[12] In this paper we show, for the first time, that mixed-phase $W_xMo_yC_zS_2$ nanotubes can be generated via pyrolysis of $H_2S$ over carbon-containing W and Mo oxide complexes.

A mixture of WC and $Mo_2C$ powders (Aldrich, U.K.), 1:1 by weight, was ultrasonicated with acetone for 30 min. The resulting dark-gray mixture was dried at 100 °C for 1 h and then heated at 700 °C in air for 10 min to partly oxidize the mixed carbides. X-ray diffraction analysis of the product revealed reflections of either individual $MO_3$ units (M = W, Mo) or a mixture of $MO_3$ with the carbides. EDX analysis confirmed the presence of W, Mo, O, and C. This mixture was transferred to a quartz boat, which was placed in a quartz glass tube (outer diameter 8 mm, inner diameter 6 mm), installed in a digitally controlled electric furnace. A flow of $N_2$/$H_2S$ (5−10:1 ratio) was passed over the mixed oxide, and the temperature was maintained at 900 °C for 30−50 min. Upon cooling, the dark product was removed from the quartz boat and submitted to electron microscopy, EDX, EELS, X-ray diffraction, and SQUID analysis.

Tube-like nanostructures (20−30% yield), with or without encapsulated materials, attached to larger irregular particles were observed by TEM (Figure 1 a−c). HRTEM revealed that these nanotubes possess a well-defined layered structure along the *c*-axis, with a *d* spacing of ≈6.2 Å (Figure 1d,e). The nanotubes exhibit polyhedral tips (Figure 1f) and range from 0.5 to 4 $\mu$m in length and 20−100 nm in diameter. EDX analysis of individual tubes showed that S, W, Mo, and C were present (Figure 2a). However, when the probe was focused on the encapsulated particles and the walls surrounding it, oxygen was also detected (insert, Figure 2a). In the EDX profile, a minor overlap between S (K-peak) and Mo (L-peak) was evident at ≈2.3 keV. An EDX line scan (mapping mode) was also carried out on a single nanotube. In this instance, S, Mo, and W were again detected (Figure 2b), but carbon was not, because of its low sensitivity in mapping analysis. Figure 2b also reveals that the W content is greater than that of Mo. Metals are well dispersed throughout the tube structure. The presence of an S−Mo overlap in the EDX profile makes estimating accurate ratios among W, Mo, C, and S difficult. However, if one ignores the minor overlap, approximately $W_{0.7}Mo_{0.2}C_{0.1}S_2$ stoichiometry is obtained. This value remains more-or-less constant in most of the observed 10 empty nanotubes. Nevertheless, the W/Mo/C/S ratio varies considerably in the nanotubes containing encapsulated materials, particularly in the tube walls near the endohedral particles. Table 1 shows approximate W, Mo, S, O, and C concentration ratios for the walls of a selected nanotube close to the encapsulated particle (Figure 2c), based on an X-ray VG-STEM analysis. Several features are distinguishable:

* To whom correspondence should be addressed.
[†] University of Sussex.
[‡] University of Cambridge.
[§] Université Paris-Sud.
[∥] Instituto de Física, UNAM.
[⊥] Max Planck Institut für Metallforschung.
[#] Instituto de Investigaciones en Materiales, UNAM.

(1) Mintmire, J. W.; Dunlap, B. I.; White, C. T. *Phys. Rev. Lett.* **1992**, *68*, 631.
(2) Falvo, M. R.; Clary, G. J.; Taylor, R. M.; Chl, V.; Brooks, F. P.; Washburn, S.; Superfine, R. *Nature* **1997**, *389*, 582.
(3) Yao, Z.; Henk, W.; Postma, Ch.; Balents, L.; Dekker, C. *Nature* **1999**, *402*, 273.
(4) Colins, P. G.; Zettl, A.; Bando, H.; Thess, A.; Smalley, R. E. *Science* **1997**, *278*, 100.
(5) Stephan, O.; Ajayan, P. M.; Colliex, C.; Redlich, Ph.; Lambert, J. M.; Bernier, P.; Lefin, P. *Science* **1994**, *266*, 1683.
(6) Suenaga, K.; Colliex, C.; Demoncy, N.; Loiseau, A.; Pascard, H.; Willaime, F. *Science* **1997**, *278*, 653.
(7) Kohler-Redlich, Ph.; Terrones, M.; Manteca-Diego, C.; Hsu, W. K.; Terrones, H.; Rühle, M.; Kroto, H. W.; Walton, D. R. M. *Chem. Phys. Lett.* **1999**, *310*, 459.
(8) Zhang, Y.; Suenaga, K.; Colliex, C.; Iijima, S. *Science* **1998**, *281*, 973.
(9) Hu, J.; Ouyang, M.; Yang, P.; Lieber, C. M. *Nature* **1999**, *399*, 48.
(10) Tenne, R.; Margulis, L.; Genut, M.; Hodes, G. *Nature* **1992**, *360*, 444.
(11) Feldman, Y.; Wasserman, E.; Srolovitz, D. J.; Tenne, R. *Science* **1995**, *267*, 222.
(12) Frey, G. L.; Elani, S.; Homyonfer, M.; Feldman, Y.; Tenne, R. *Phys Rev B* **1998**, *57*, 6666.

10.1021/cm0011256 CCC: $19.00 
Published on Web 11/10/2000

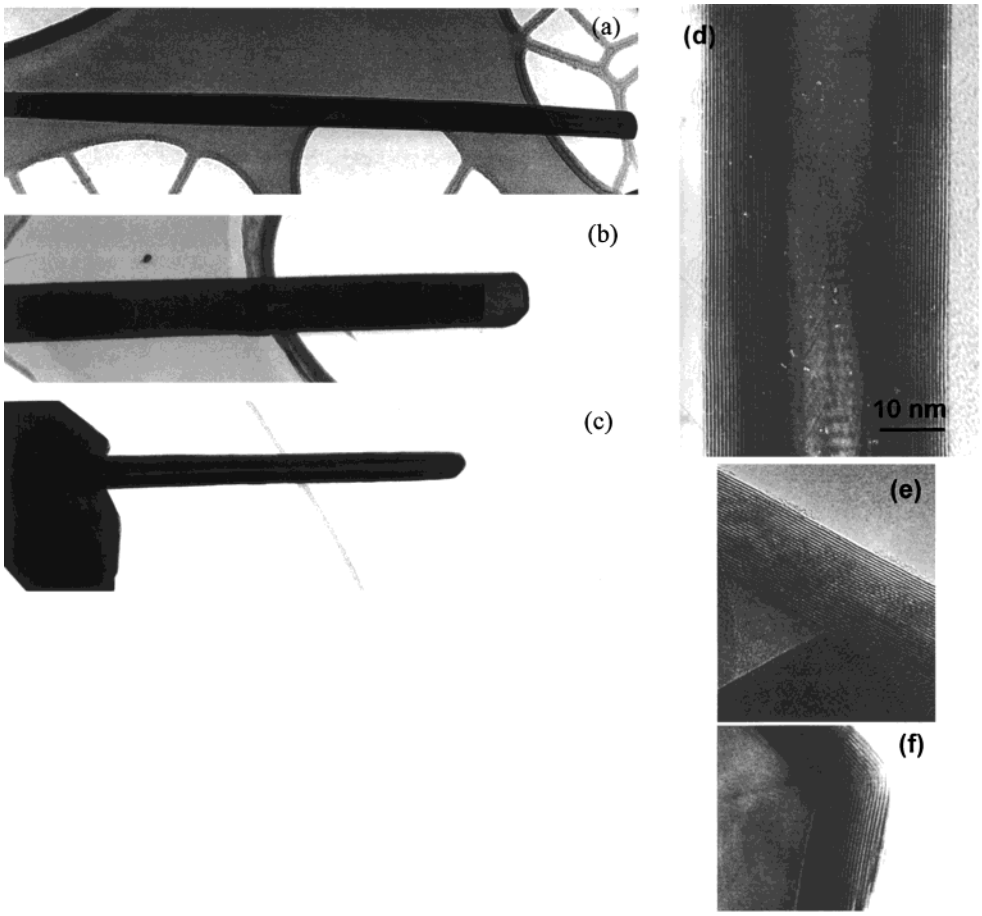


**Figure 1.** TEM images of $W_xMo_yC_zS_2$ nanotubes (a), an encapsulated nanotube (b), a nanotube connected with a irregular oxide particle (c), HRTEM image of a nanotube (d), and the tube walls near endohedral particle (e), and the polyhedral nanotube tips (f).

(a) An increase in carbon content (up to 31%), as compared with the empty nanotubes, but limited along the tube axis between the tube and encapsulated particle (position a to position c). (b) 31% oxygen content is detected in the tube walls, associated with an endohedral particle (i.e., position c) which reduces rapidly to ≈1%, as the distance from the particle increases (i.e., positions a and b). (c) The relatively low S content (10%) in position c increases rapidly to 46% as the distance from the encapsulated particle increases. (d) The Mo content is also relatively low, in all positions, as compared with the empty nanotubes. (e) In position b, the W content falls, and the W/Mo ratio approaches 2:1. (f) The W content is always greater than Mo. (g) The O/S ratios in both regions (i.e., a−b and c) are anticorrelated; that is, if S increases, O decreases, and vice versa. On the basis of Table 1, the stoichiometry of the encapsulated tube (Figure 2c) varies from $W_{0.38}Mo_{0.07}C_{0.55}S_2$ (position a), $W_{0.32}Mo_{0.16}C_{0.49}S_2$ (position b), to $W_{0.26}Mo_{0.02}C_{0.3}O_{0.3}S_{0.1}$ (position c), and the oxygen content in positions a and b is negligible. EDX-mapping (Figure 2d) and high spatial resolution line scans analyses (Figure 2e) were also carried out to obtain further information regarding elemental distribution across the tube walls in Figure 2c. Figure 2d shows the mapping images of O, W, Mo, and S. It is clear from this Figure that (a) the oxygen content is greater in the encapsulated oxide than in the tube walls. (b) The S content mainly arises from the tube walls; a trace is also discernible in encapsulated oxide. (c) The high W content remains almost identical in positions a and c, but decreases rapidly in position b. (d) A trace of Mo, observed in positions a and c, increases rapidly in position b. In Figure 2e, S is mainly distributed in the tube walls. On the other hand, W is dispersed evenly, both in the tube walls and in the encapsulated particle. In position c, Mo is found mostly in the tube walls. However, Figure 2e is consistent with Figure 2d and Table 1. Although the variation in the elemental ratio is apparent, HRTEM showed the presence of well-defined layered structures in the tube walls near the encapsulated particles (Figure 1e).

In a traditionally layered $MS_2$ system (M = Mo or W),[10,11] individual $MS_2$ shells consist of a metal layer sandwiched between two sulfur layers (i.e., S−M−S). The S atoms bond to the metal atoms, to the exclusion of M−M or S−S bonds. Despite the encapsulated oxide, the existence of carbon in the tube walls is interesting, particularly with regard to the way carbon bonds to the $MS_2$ structure. The C-intercalated $MS_2$ structure is unlikely[13] because the layer separation along the *c*-axis only varies within ±0.05 Å, as indicated by HRTEM. Partial replacement of W atoms by Mo, and vice versa, is possible (i.e., lattice substitution) because of their similar lattice constants and identical oxidation state. This will result in the formation of a $W_xMo_yS_2$ structure ($x + y = 1$). In our study, the individual layers with

(13) Remškar, M.; Škraba, Z.; Stadelmann, P.; Lévy, F. *Adv. Mater.* **2000**, *12*, 814.

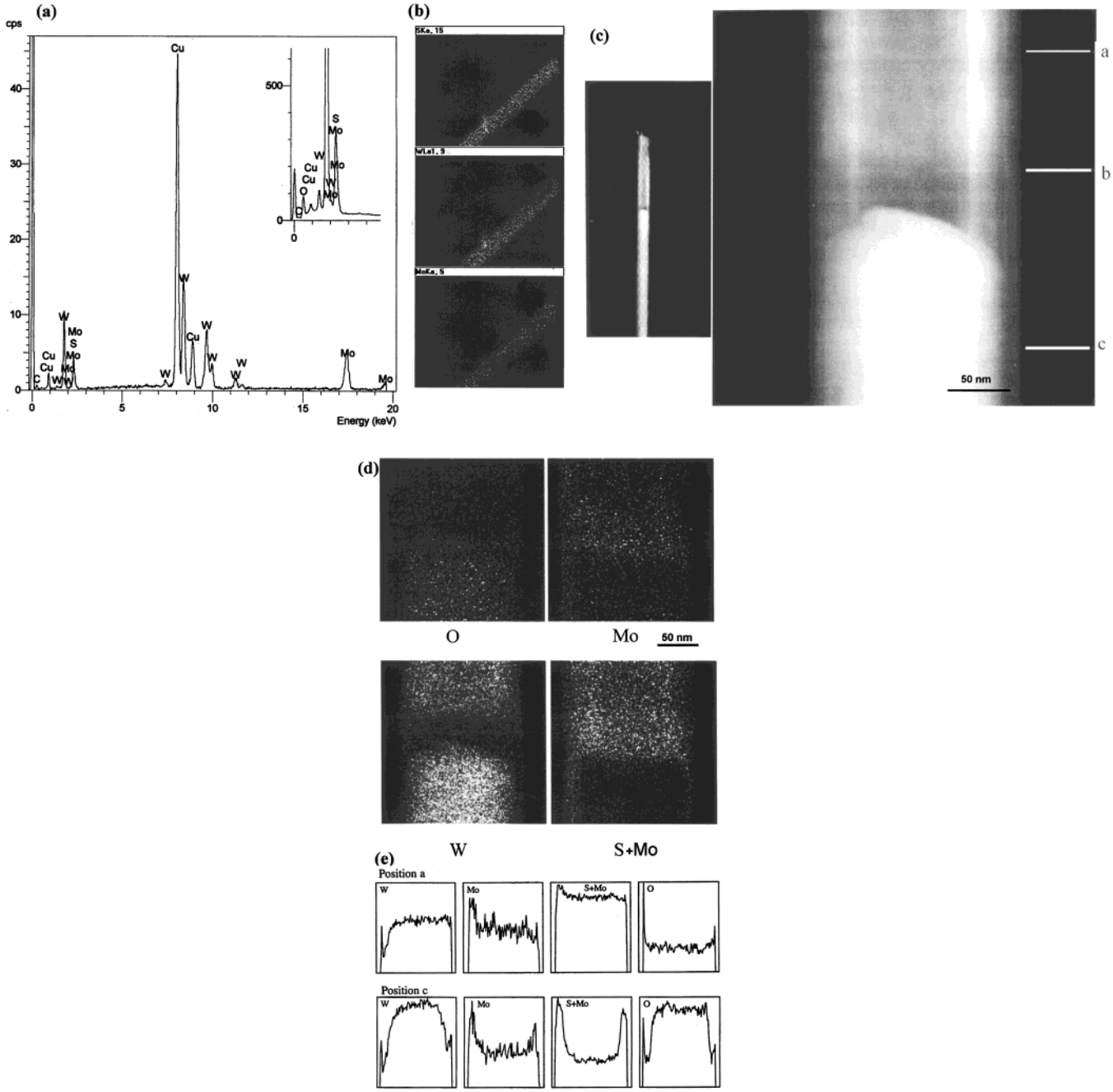


**Figure 2.** (a) EDX analyses of an empty $W_xMo_yC_zS_2$ nanotube, showing the presence of W, Mo, C, and S signals from the tube walls. Oxygen is present in the tube walls in conjunction with encapsulated oxide (insert). (b) Mapping analyses of a $W_xMo_yC_zS_2$ nanotube, S (top), W (middle), and Mo (lower) are clearly seen. The energy count was taken from S (Ka-shell), W (La-shell), and Mo (Ka-shell), respectively. (c) Dark-field image of an encapsulated tube (left). Line scans analyses across the tube, along positions a, b, and c (right, enlarged image). (d) EDX-mapping analyses of the same nanotube (Figure 2c). (e) EDX line scans across the tube (Figure 2c) at positions a and c.

**Table 1. Elemental Analyses of a Single Encapsulated Tube (Figure 2c), Based on X-ray VG- STEM Analysis**

| Approximate Concentration from X-ray Spectra (%) | | | |
|---|---|---|---|
| | positions | | |
| elements | a | b | c |
| W | 21 | 17 | 26 |
| Mo | 4 | 8 | 2 |
| S | 44 | 46 | 10 |
| O | 1 | 1 | 31 |
| C | 30 | 28 | 30 |

6.2-Å separation, revealed by HRTEM (Figure 1d−f), also exhibit the S−M−S structure (M = $Mo_xW_yC_z$ in this case). It is unlikely that an alternating layered stacking along the *c*-axis, for example, SWS/SMoS/SWS, or a small Mo domain incorporated into the W-lattice occurs on the basis of the line scan analyses (Figure 2e). The precursor consisted of partly oxidized metal carbide, and after the S substitution, a small quantity of interstitial carbide—either WC or $Mo_2C$—may be preserved, particularly in the tube walls near the encapsulated particle, as a relatively high carbon content is found (Table 1 and Figure 2c). In Figure 3, a nanotube with an encapsulated particle was selected for EELS line scan analysis (position denoted by arrow). S, Mo, and C were detected and, in this case, Mo−C is found in the tube walls.

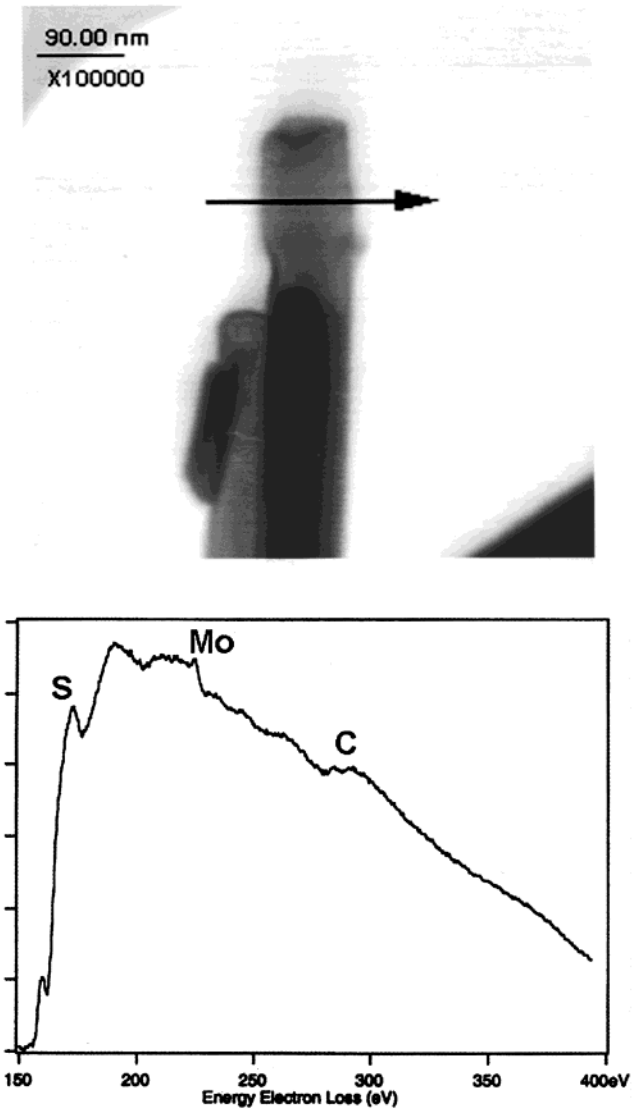


**Figure 3.** EELS analyses of an encapsulated tube tip (top, arrow). S (165 eV), Mo (227 eV), and C (285 eV) are discernible (lower), after the background subtraction. W was unable to be scaled in this case; therefore, the presence of W cannot be ruled out.

An X-ray diffraction study shows that our $W_xMo_yC_zS_2$ sample does not differ from the 2H−$MS_2$ system (Figure 4a), indicating that the presence of carbon does not bring about significant changes in the 2H−$MS_2$ skeleton. Two possible structures account for the presence of C in $MS_2$. The first involves the appearance of so-called "misfit compounds";[14] in this case either the $WS_2$ and WC, or $MoS_2$ and MoC, are arranged in an alternating layered structure, that is, $MS_2$/MC/$MS_2$. The long-range order in such a structure can still be maintained.[14] Second, the carbon is bonded to the metal atoms (M−C structure), for example, Figure 4b. This structure is supported by the following observations: (a) the presence of S−C bonds (i.e., C is situated within the S layers) is unlikely because of the invariable oxidation state of S in the 2H−$MS_2$ system. (b) The trigonally hybridized carbon may fit reasonably well within a $MS_2$ trigonal-prism cell. (c) The change of coordination number, from six for M to nine for M−C, lies well within the range of a metallic crystal model.[15] (d) During S substitution, O is replaced and carbide remains, for example, Figure 3. In this context, the carbide should retain its initial structure or be only a slightly distorted interstitial structure.

Recently, Feldman et al. suggested that the growth of $MS_2$ nanostructures involves the replacement of oxygen by sulfur to form $MS_2$ layered structures on the surface of the oxide.[16] The rapid formation (ca. 2 s) of one or two $MS_2$ layers inhibits the fusion of adjacent oxide particles. $H_2S$ then begins to diffuse through the $MS_2$ layers via defects (vacancies or dislocations) toward the center of the particles. In this case, the initial morphology of $MO_3$ determines the formation of fullerene-like $MS_2$ nanostructures; that is, a template effect operates. If $MO_3$ precursors could be converted into nanoparticles before S substitution occurs, generation of fullerene-like nanomaterials would be probable. However, it appears that this template effect may not apply to $W_xMo_yC_zS_2$ nanotube formation because TEM investigations showed that more than 90% of the original oxide complexes were large, irregular particles (>1 $\mu$m), for example, Figure 1c. Nevertheless, the inward growth process remains valid because of the presence of the encapsulated oxide inside $W_xMo_yC_zS_2$ nanostructures.[17] During S substitution at an elevated temperature, the oxide crystallites rapidly disintegrate into small particles, which form $W_xMo_yC_zS_2$ nanoparticles.[18] Change of oxide morphologies in favor of anisotropic growth (i.e., nanotube formation) may occur in the presence of a temperature gradient across the oxide particles,[19] particularly at the crystal facets.[20]

In the $H_2S$−$MO_3$ reaction (M = Mo, W), M and O atoms must have changed their valency and configuration to form $MoS_2$ layered structures. For example, the oxidation state for Mo in an orthorhombic phase $MoO_3$ oxide crystallite[15] is $M^{VI}$ ($d^0$), which changes into $M^{IV}$ ($d^2$) as $MoS_2$ forms. Direct conversion of $MoO_3$(s) into $MoS_2$(s) is unlikely because of the energy barrier. Therefore, an intermediate structure, which stoichiometrically approximates to $MoS_2$, to some extent, is possibly involved (e.g., $MoO_2$).[18] Feldman et al. also suggested that an excess of $H_2$ (i.e., reducing agent) is essential to form an intermediate structure, $MoO_{3-x}$, prior to $MoS_2$ formation.[11] Accurate control of the reducing atmosphere at elevated temperature is crucial in determining the chemical route from $MoO_{3-x}$ to (a) orthorhombic $MoO_{2-x}S_x$, (b) amorphous $MoS_3$, or (c) 2H−$MoS_2$.[11] The significance of $MO_{3-x}$ lies in a gas-phase reaction between $MoO_3$(s) and $H_2S$ via the volatile $MoO_{3-x}$(g) species. In our study, the transformation of the oxide precursor into a $MS_2$-type layered structure

(14) Hoistad, L. M.; Meerschaut, A.; Bonneau, P.; Rouxel, J. *J. Solid State Chem.* **1995**, *114*, 435.

(15) Hulliger, F. *Structural Chemistry of Layer-Type Phases*; Lévy, F., Ed.; D. Reidel Publishing Co.: Dordrecht, 1976; pp 3−5, 171−173.

(16) Feldman, Y.; Frey, G. L.; Homyonfer, M.; Lyakhovitskaya, V.; Margulis, L.; Cohen, H.; Hodes, Hutchison, J. L.; Tenne, R. *J. Am. Chem. Soc.* **1996**, *118*, 5362.

(17) Sloan, J.; Hutchison, J. L.; Tenne, R.; Feldman, Y.; Tsirlina, T.; Homyonfer, M. *J. Solid State Chem.* **1999**, *144*, 100.

(18) Feldman, Y.; Lyakhovitskaya, V.; Tenne, R. *J. Am. Chem. Soc.* **1998**, *120*, 4176.

(19) Oberlin, A.; Endo, M.; Koyama, T. *J. Cryst. Growth* **1976**, *32*, 335.

(20) Grobert, N.; Terrones, M.; Osborne, A. J.; Terrones, H.; Hsu, W. K.; Trasobares, S.; Zhu, Y. Q.; Hare, J. P.; Kroto, H. W.; Walton, D. R. M. *Appl. Phys. A* **1998**, *67*, 595.

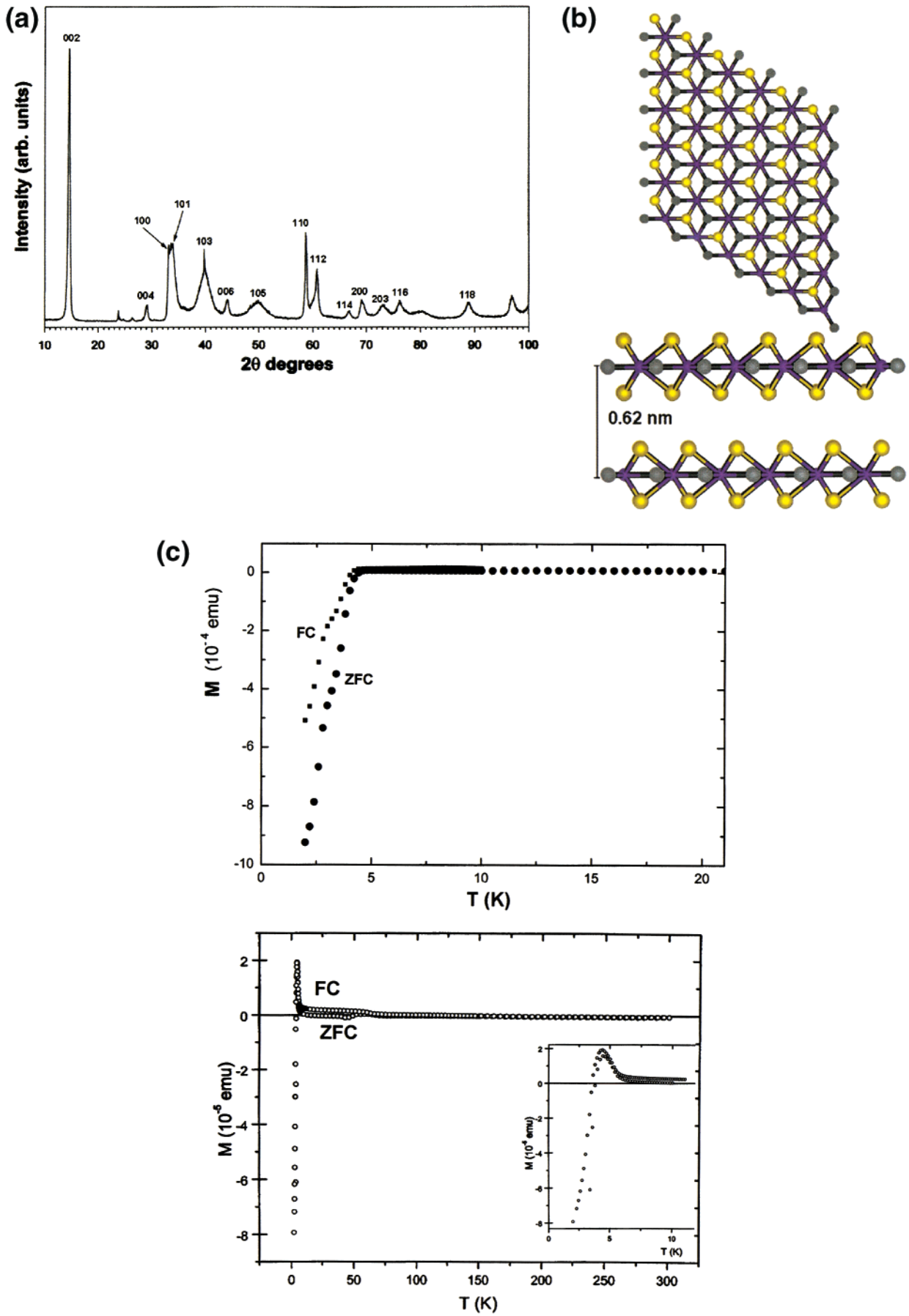


**Figure 4.** (a) X-ray diffraction of $W_xMo_yC_zS_2$ product, showing no significant difference from that of 2H−$MS_2$ structures (2H: two 3-fold symmetry in a hexagonal cell, M = W, Mo; see also ref 26). (b) $W_xMo_yC_zS_2$ structure, viewed along the *c*-axis (top) and in-plane (lower). Carbon atoms (gray) locate within the metal layer, bonded to the metal atoms (purple), S atoms (yellow). (c) SQUID measurement of oxide precursor (top) and $W_x$-$Mo_yC_zS_2$ nanotubes (lower). Both exhibit a temperature transition at ≈4.2 K. Paramagnetism appears in $W_xMo_yC_zS_2$ nanotube product at ≈6 K.

may be more complicated because of (a) the complex precursor $W_xMo_yC_zO_3$ ($x + y + z \sim 1$), (b) the presence of small quantities of a carbide structure, and (c) an excess of $H_2$ which was not involved in the reaction. The only reducing agent arises from the decomposed $H_2S$, the hydrogen subsequently reacting with the metal oxide to form $H_2O$. However, small quantities of carbon or carbide also have the same effect as $H_2$ in reducing the oxide to form $CO_2$. In this respect, the formation of an intermediate structure in our process is minor, implying that direct transformation between the oxide precursor and layered structure products is likely to have occurred. Our oxide precursor possibly consists of large domains of orthorhombic $MO_3$ ($M = W_xMo_y$, $x + y = 1$), interconnected by small amounts of interstitial carbide, as revealed by X-ray diffraction. In fact, the orthorhombic $MO_3$ has a layerlike alternating structure (O−M−O) when viewed along the *b*-axis,[15] which has advantages over the formation of layered 2H−$MS_2$ nanostructures. The distance between the upper and lower oxygen layers is ≈4 Å, a value which facilitates $H_2S$ diffusion. We therefore conclude that the formation of layered $W_xMo_yC_zS_2$ may commence with the oxide precursor along the *b*-axis. During S substitution, W, Mo, and the remaining carbide can be simultaneously incorporated into the lattice. The variation in elemental ratios detected in the tube walls near the endohedral oxide (Figure 2c,d and Table 1) remains unclear at this stage. However, the different oxide volatilities (i.e., $WO_3$ and $MoO_3$) result in $WS_2$ and $MoS_2$ nanostructures forming at different rates;[16,18] the former is favored in solid−gas reactions and the latter in gas-phase reactions. When the generation of $W_xMo_yC_zS_2$ begins at the surface of the oxide precursor, the growth rates of $WS_2$ and $MoS_2$ differ. This difference could well account for the observed variation in the W/Mo/C/S ratio in the tube walls, associated with the endohedral particles. Because $MoO_3$ is more volatile than $WO_3$, the excess of W in the nanotube walls is to be expected, as is consistent with data in Table 1. By contrast, heating mixtures of yellow $WO_3$ and $MoO_3$ powders (Aldrich, U.K.) did not result in $W_xMo_yC_zS_2$ nanotubes, but generated either individual $WS_2$ or $MoS_2$ nanoparticles. This result may be due to the absence of residual carbide linking individual tungsten and molybdenum oxides, the sulfides being miscible only when nonstoichiometric, that is, $WS_{2-x}$.

It has been shown that inorganic layered materials (e.g., $TaS_2$, $NbSe_2$) exhibit superconducting behavior.[21,22] To date, the presence of superconducting inorganic fullerene-like nanomaterials (e.g., $WS_2$ and $MoS_2$) remains to be established. Interstitial carbides, WC and $Mo_2C$, superconduct at 5.89[23] and 10.5 K,[24] respectively. In our study, the carbon-containing oxide precursor also superconducts at ≈4.2 K, possibly arising from the residual WC, for the following reasons. First, the W content is always greater than the Mo content in our study. Second, the detected transition temperature is consistent with a bulk phase of WC. Third, only 2−3% of the material superconducts. In other words, superconducting behavior arising from the major oxide ($MO_3$: $M = W_xMo_y$) is unlikely. Moreover, tungsten or molybdenum oxides do not superconduct, except when intercalated with alkali metals (Na).[25] The $W_xMo_yC_zS_2$ nanotubes are insulators at room temperature, according to resistance measurements. The superconducting phase reappears at ≈4.2 K and originates from two regions: encapsulated oxide particles and the tube walls, both of which contain WC. Meanwhile, a positive magnetization, corresponding to paramagnetism, is also present at 6 K (Figure 4c), which then rapidly switches to the superconducting phase. The paramagnetism exhibited by $W_xMo_yC_zS_2$ at low temperature most probably arises from the tube walls, not the encapsulated oxides. This assumption is based upon the inward growth model; if S substitution begins at the oxide surfaces, then the encapsulated oxides, due to incomplete reaction, should retain the same structure and stoichiometry as the initial oxide precursor, which is not paramagnetic. The occurrence of "Curie-tail" paramagnetism in $W_xMo_yC_zS_2$ nanotubes at low temperature is currently under investigation.

**Acknowledgment.** We thank the EPSRC (W.K.H.), Royal Society (N.G.), the Japan Fine Ceramic Centre (Y.Q.Z.), and DGAPA-UNAM and CONACYT (25237-E and J31192-U) (H.T., M.T.) of Mexico for financial support. We also thank J. Thorpe and D. Randall (Sussex) for providing valuable assistance with the electron microscopy.

CM0011256

(21) Nagata, S.; Aocht, T.; Abe, T.; Ebisu, S.; Hagino, T.; Seki, Y.; Tsutsumi, K. *J. Phys. Chem. Solids* **1992**, *53*, 1259.

(22) Morales, J.; Santos, J.; Baas, J.; Wiegers, G. A.; Matinez, J. L. *Chem. Mater.* **1999**, *11*, 2737.

(23) Rajagopalan, M.; Saigeetha, P.; Kalpana, G.; Palanivel, B. *Jpn. J. Appl. Phys.* **1994**, *33*, 1847.

(24) Terrones, M.; Hsu, W. K.; Schilder, A.; Terrones, H.; Grobert, N.; Hare, J. P.; Zhu, Y. Q.; Schwoerer, M.; Prassides, K.; Kroto, H. W.; Walton, D. R. M.; *Appl. Phys. A* **1998**, *66*, 307.

(25) Reich, S.; Tsabba, Y. *Eur. Phys. J. B* **1999**, *9*, 1.

(26) Zhu, Y. Q.; Hsu, W. K.; Grobert, N.; Chang, B. H.; Terrones, M.; Terrones, H.; Kroto, H. W.; Walton, D. R. M. *Chem. Mater.* **2000**, *12*, 1190.